

Analysis of the heat losses associated with the SAGD visualization experiments

Omid Mohammadzadeh¹ · Ioannis Chatzis²

Received: 25 May 2015 / Accepted: 2 August 2015 / Published online: 15 August 2015
© The Author(s) 2015. This article is published with open access at Springerlink.com

Abstract Dealing with the heat losses associated with steam-assisted gravity drainage (SAGD) experiments has been an issue for which different heat loss prevention techniques have been developed and utilized in the literature. The aim is to minimize the amount of heat losses from the porous medium to the surrounding environment. Excessive heat losses negatively affect quantifying the energy requirements of the SAGD experiments. In this study, an inverted-bell vacuum chamber was employed to minimize the excessive heat losses while steam was injected under different superheating levels. Local temperatures along the glass micromodels' height and width were recorded on a real time basis. Details of the heat losses associated with our pore-scale SAGD visualization experiments are described in this paper. According to the results presented, employing extremely low vacuum conditions resulted in effective heat loss prevention in a sense that the convective element of heat loss could be neglected. As a result, radiation heat transfer was the only mechanism of heat transfer that contributed to the heat loss from the micromodels' surfaces. In each pore-level SAGD experiment, the overall steam consumption to produce one unit of the mobile oil was corrected based on the heat loss analysis of the process to account for the additional volume of steam which was condensed because of the heat loss. The net cumulative steam consumed, corrected for the heat losses, was in very good agreement with the predictions

made based on the theory of gravity drainage and its application in performance analysis of the SAGD process.

Keywords Bitumen · Convection heat transfer · Heat loss · Porous media · Radiation heat transfer · Steam-assisted gravity drainage

List of symbols

Variables and parameters

CWE (m ³)	Cold water equivalent
C_p (J kg ⁻¹ K ⁻¹)	Specific heat capacity
CSOR (m ³ /m ³)	Cumulative steam to oil ratio
d (m)	Diameter
F_{12} (dimensionless number)	View factor
H (J kg ⁻¹)	Enthalpy
k_B (W m ⁻² K ⁻⁴)	Stefan–Boltzmann constant
Kn (dimensionless number)	Knudsen number
L (m)	Length
\dot{m} (kg s ⁻¹)	Mass flow rate
MW (g mol ⁻¹)	Molecular weight
n (m ⁻³)	Gas number density
N_A (mol ⁻¹)	Avogadro's number
p (Pa)	Pressure
q_{12} (W)	Net radiation exchange between the two surfaces
\dot{Q}_{loss} (W)	Heat losses to the surrounding environment
SOR (m ³ /m ³)	Steam to oil ratio
T (°C)	Temperature
W (m)	Width

Greek letters

λ (m) Mean free path

✉ Omid Mohammadzadeh
omohamma@uwaterloo.ca

¹ DBR Technology Centre, Schlumberger, 9450, 17 Ave.,
Edmonton, AB, Canada

² Department of Chemical Engineering, University of
Waterloo, 200 University Ave. W, Waterloo, ON, Canada

λ (kJ/kg)	Latent heat of condensation
ϵ	Emissivity of a particular surface
σ ($\text{W m}^{-2} \text{K}^{-4}$)	Stefan–Boltzmann constant

Subscripts

in	Inlet face
out	Outlet face
S	Steam or steam temperature
Sat	Saturation state
SC	Sub-cooled
Steam	Steam phase

Superscripts

L	Liquid
S	Steam phase
vap	Vapour
W	Water phase

Introduction

The SAGD process is considered as one of the most prominent bitumen recovery methods. This method was theoretically developed, pilot tested, and commercialized in Canada and has been successfully implemented at the field-scale in Canada and Venezuela. With recent advancements in horizontal well drilling, monitoring the in situ processes, and reliable modelling of the field-scale performance, very high recovery rates and economical steam-to-oil ratios are achievable. The macro-scale performance of the SAGD process was extensively investigated in the literature using scaled physical models of porous media (Butler 1987, 2004). Attempts were made recently to elucidate the pore-scale physics of the SAGD process and its solvent-aided modification for the first time in the literature with the aid of direct visualization experiments using glass-etched micromodels of porous media (Mohammadzadeh 2012; Mohammadzadeh and Chatzis 2010; Mohammadzadeh et al. 2010, 2012, 2015).

In the SAGD process, two horizontal wells are drilled parallel to each other and are completed near the base of the pay zone with a vertical spacing of 5–7 m from each other. Steam is injected under constant injection pressure through the upper well, while water condensate and draining mobile oil are produced on a continuous basis from the lower production well (Butler et al. 1979, 1981). The schematic diagram presented in Fig. 1 is a vertical cross-section of the SAGD scheme, perpendicular to the horizontal extension of the paired horizontal wells. Oil movement towards the producer is caused by the resultant action of gravity and capillarity forces. Injected steam forms a continuously growing steam-saturated zone called “steam chamber”, which is the interface between the hot steam and cold bitumen. Steam condenses at the

boundaries of the steam chamber, hence giving the latent heat of condensation to the cold bitumen that reduces its viscosity. The mobile oil and water condensate move approximately parallel to the steam chamber/bitumen interface towards the producer. Using this recovery technique, bitumen can be extracted in a systematic manner with very high ultimate recovery factor values which are significantly greater than those achieved using the conventional steam flooding processes.

The original concept of the SAGD process was proposed by Butler and his colleagues in late 1970s, taking advantage of the traditional steam flooding experiences and the newly developed horizontal well technology. The novel idea behind the SAGD process was developed and modified by Butler and his associates in a number of publications (Butler et al. 1979, 1981; Butler and Stephens 1981; Butler 1991, 1994a, b, 1998, 2001). The macro-scale performance of the SAGD process has been extensively investigated in the literature with the aid of scaled physical models, and heat loss preventive techniques were broadly used in these studies to make the energy requirements of this process more reliable. The energy intensity of a thermal process of heavy oil and bitumen recovery is defined as the volume of steam, in terms of its cold water equivalent (CWE), which is needed to produce one unit volume of the mobile oil. This production characteristic of the SAGD process, which also specifies the economics of this thermal recovery method, is called the cumulative steam to oil ratio (CSOR). In the presence of heat losses, more steam would be consumed, to cover in part the undesired heat losses across the porous medium boundaries, than the volume which is truly needed to facilitate the gravity drainage process. The boundaries of the porous medium should be considered no flow in terms of heat and mass so that reliable amounts of CSOR would be obtained. In most of the conceptual designs proposed in the literature, layers of insulating materials were used to reduce the heat losses from the porous medium boundaries. Very effective insulating materials such as Pyrogel[®] XT are now being manufactured which are very efficient in creating a no heat flow boundary across the porous models. The outer walls of these physical models can also be manufactured using thick Polycarbonate Plexiglas[®] or Teflon[®] polytetrafluoroethylene (PTFE) sheets because of their low thermal conductivity, high operating temperature rating, and enhanced compressive strength. A schematic diagram of a cross-sectional packed prototype of porous media which is sandwiched between two parallel thermal insulation layers is depicted in Fig. 2.

In this paper, the novel use of vacuum environment to reduce the heat losses during the SAGD visualization experiments is presented. In this study, a series of pore-scale SAGD visualization experiments were conducted

Fig. 1 Conceptual flow diagram of the SAGD process

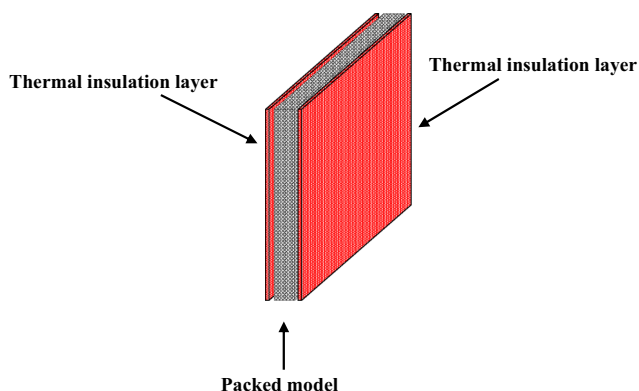
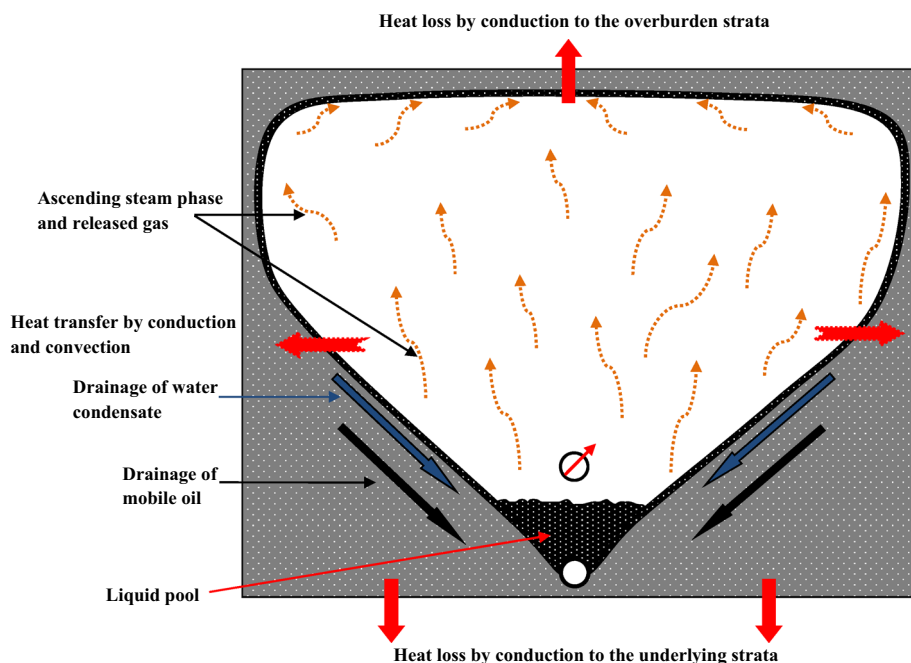


Fig. 2 Schematic representation of a rectangular packed model sandwiched between two parallel insulation layers

under controlled environmental conditions of very low vacuum pressure. Micromodels of capillary networks etched on glass plates were developed, fabricated and then saturated with bitumen at lab conditions. A high-precision inverted-bell vacuum chamber was used to minimize the heat losses from the glass-etched micromodels to the surrounding environment while steam was injected under different superheating levels. Local temperatures along the glass micromodels' height and width were recorded on a real time basis. The pore-scale events were video recorded during the visualization experiments; digital images were then reproduced and analyzed using image processing techniques and finally, the pore-scale events were documented. Details of the pore-scale analysis of the recovery mechanisms, flow behaviour and fluid flow of the SAGD

experiments are presented elsewhere (Mohammadzadeh 2012; Mohammadzadeh and Chatzis 2010). In this paper, details of the heat loss analysis associated with our pore-scale SAGD visualization experiments are described.

Experimental setup

Pore-scale visualization experiments of the SAGD process suffer from the excessive heat losses from the model (i.e. at steam temperature) to the surrounding environment (i.e. at lab temperature). As a result of this heat loss, a considerable fraction of the injected steam, which is supposed to condense on the cold face of bitumen, would then condense to make up for the above-mentioned temperature difference. To facilitate an effective steam heating of the bitumen-saturated micromodel in the absence of an undesired heat loss, a high-precision vacuum test rig, capable of providing 10^{-6} torr of vacuum pressure was used as is depicted in Fig. 3. As is seen in this snapshot, a glass micromodel saturated with bitumen was secured at the centre of the inverted-bell jar using a model holder. The superheated steam was injected from the top into the model, and the draining water condensate as well as the mobile oil was produced from the bottom production hole in the model. A steam-saturated zone was initiated and then developed laterally in the micromodel while oil drained out of the porous medium. As a result, the area available for heat loss gradually expanded versus time.

The properties of bitumen used in the pore-scale SAGD experiments are presented (Table 1; Figs. 4, 5). Here, it is

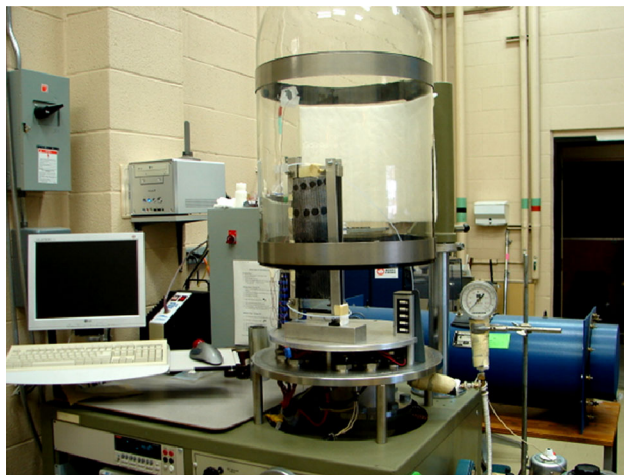


Fig. 3 A snapshot of the employed vacuum test rig

Table 1 The physical properties of Cold Lake bitumen

Density versus temperature	
Bitumen density (g/cc)	Temperature (°C)
1.012	15
1.001	22
0.997	40
0.978	70
SAPA analysis	
Fraction	Mass (%)
Saturates	22.4
Aromatics	30.8
Polars	29.4
Asphaltenes	17.4
Main elemental characterization	
Element	Mass percent
Carbon	83.62
Hydrogen	9.57
Nitrogen	0.39
Sulphur	5.25
Viscosity at 30 °C	47,000 cp
Molecular weight	557 g/mol

not intended to describe the flow system and experimental setup associated with the pore-scale SAGD experiments; instead, we are focusing on the heat loss prevention technique used in this setup in the form of the environmental vacuum chamber. This vacuum chamber operated with a combination of a mechanical and a diffusion pump. All the visualization tests were carried out at the vacuumed environment within the pressure range of 5×10^{-6} – 10^{-4} torr.

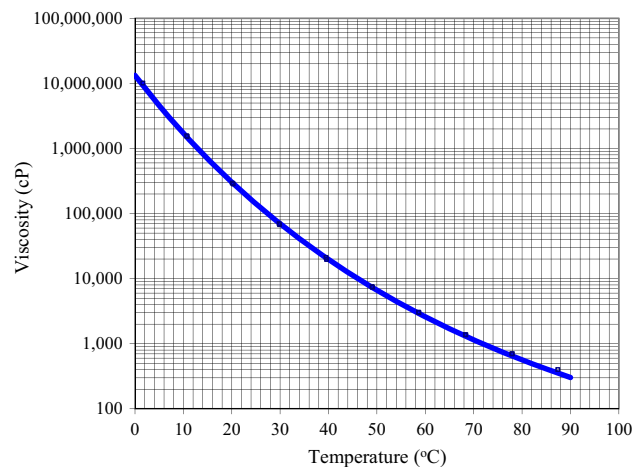


Fig. 4 Viscosity–temperature relationship for Cold Lake bitumen

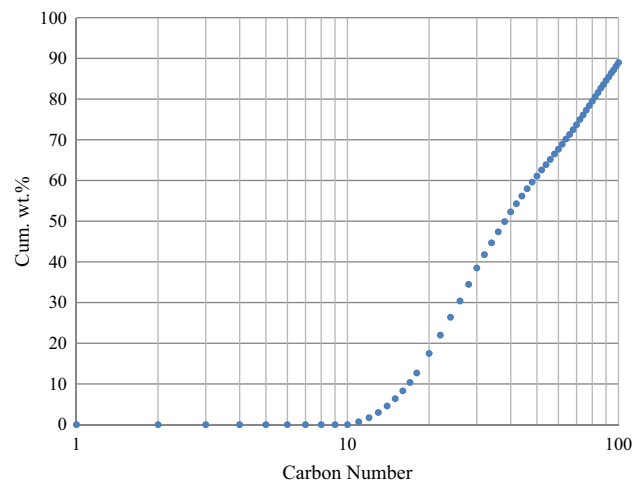


Fig. 5 C_{100} hydrocarbon analysis for Cold Lake bitumen

According to the heat loss calculations presented later in this paper, it is believed that the amount of heat loss from the glass surface to the surrounding environment by convection mechanism was negligible at this very low range of air pressure. At this low magnitude of vacuum pressure, the only important heat loss mechanism is the radiation heat transfer. This heat transfer mechanism was also lowered by covering the hot spots of the micromodels with shiny reflective thin films such as strips of aluminum foil. In addition, the portions of the inverted bell jar, which were not needed from the visibility point of view, were covered with aluminum foil. Operating the SAGD experiments at low values of environmental air pressure not only prevented the steam phase to condense as a result of excessive undesired heat loss, but also allowed the steam phase to transfer its latent heat of condensation to the cold bitumen face where it was supposed to do so.

Table 2 Physical and pore-scale characteristics of the glass micromodels

Model name	DC1	DL1	OC-1	OM1	OM2
Physical dimensions					
Length (mm)	304.00	304.00	304.00	301.00	301.00
Pattern length (# of pores)	190	149	149	150	150
Width (mm)	141.00	100.00	100.00	101.00	101.00
Pattern width (# of pores)	89	49	49	50	50
Pore-scale dimensions					
Depth of etching ^a (μm)	127.70 ± 0.80	250.20 ± 0.90	125.3 ± 1.7	118.90 ± 1.70	196.80 ± 6.60
Pore body width (mm)	1.31	2.04	1.38	2.00	2.00
Pore throat width (mm)	0.49	0.67	0.45	0.30	0.30
Particle size (mm)	1.11	0.99	1.59	1.20	1.20
Petrophysical properties					
Permeability (D)	34.13 ± 1.02	94.61 ± 2.49	56.16 ± 3.10	77.83 ± 4.85	92.42 ± 3.74
Porosity (fraction)	0.37	0.32	0.42	0.30	0.32

^a Depth of etching at the pore body space

Five different glass-etched micromodels were used in our pore-scale SAGD visualization experiments. These micromodels were fully characterized in terms of microscopic as well as macroscopic dimensional properties (Table 2). The surface temperatures of each model at different locations were measured on a real time basis using a series of surface thermocouples and were recorded continuously using a data acquisition system. The temperature of the glass bell jar of the vacuum chamber at the inner side was also measured at different locations and was recorded on a real time basis.

Analysis of the heat loss during the pore-scale SAGD experiments

In our pore-level SAGD experiments, the overall heat loss to the surrounding environment consisted of two elements: heat loss by convection as well as heat loss by radiation. Based on the experimental results presented in this paper, it is believed that the extremely low values of the vacuum pressure enabled us to minimize the convective heat loss to the extent that it could be ignored compared to the radiation heat loss. A heat balance was carried out for all the employed micromodels based on the range of operational conditions examined in our visualization experiments. The overall heat balance for each glass micromodel under experimental conditions of each SAGD test was used to calculate the associated energy requirements. Continuous tracking of the SAGD interface at the pore-scale enabled us to determine the amount of steam which was condensed as a result of heat loss at each particular stage of the process. Consequently, the net CSOR was calculated for each SAGD experiment.

Convective heat loss prevention using extremely-low vacuum conditions

Heat loss increases the energy requirements of a thermal recovery method in the context of increased need to heat carrying agent. Ignoring the heat losses occurred during the SAGD experiments adversely affects the quantitative and qualitative results acquired due to the excessive steam condensation. During drainage of the mobile oil from an experimental model in the SAGD process, the overall heat loss increases with time (i.e. the more oil drains out of the model, the more depleted area is available for the heat loss). Use of an effective vacuum environment can significantly limit different heat transfer mechanisms. For instance, a vacuum pressure of 0.01 torr or less is required for significant reduction of the heat loss through conduction mechanism (Roth 1990). Moreover, to establish an insulating vacuum jacket for minimizing convective element of the heat transfer, it is required to achieve an extremely low vacuum pressure of about 1×10^{-6} torr (Guyer 1999).

In gas dynamics, the ratio of the molecular mean free path “ λ ” to some characteristic length “ L ” is a measure of a dimensionless number so called Knudsen number which characterizes the approach upon which the fluid properties are calculated. The magnitude of Knudsen number also determines the appropriate gas dynamic regime. When Knudsen number is small compared to unity (i.e. $Kn \leq 0.1$), the fluid can be treated as a continuous medium and described in terms of the macroscopic variables such as velocity, density, pressure, and temperature. In the transition flow regime, for Knudsen numbers of the order of unity or greater, a microscopic approach is required, wherein the trajectories of individual representative

molecules are considered, and macroscopic variables are obtained from the statistical properties of their motions. In both internal and external flows, for $Kn \geq 10$, intermolecular collisions in the region of interest are much less frequent than molecular interactions with solid boundaries, and can be ignored. Flows under such conditions are termed collision-less or free molecular. In the range of $0.1 \leq Kn \leq 1.0$, which is known as the slip flow regime, it is sometimes possible to obtain useful results by treating gas as a continuum, but allowing for discontinuities in velocity and temperature at the solid boundaries (Gird 1994). The characteristic length chosen will depend on the problem under consideration. In our system of a glass micromodel at the centre of an inverted-bell type of vacuum chamber, the characteristic length was the distance between the glass micromodel and the glass wall of the inverted-bell chamber.

In physics, the mean free path of a particle is the average distance covered by the particle between successive similar collisions with other moving particles such as elastic collisions of molecules in a gas phase. For an ideal gas system, it can be calculated using the following equation:

$$\lambda = \frac{k_B T}{\sqrt{2} \pi d^2 p} \quad (1)$$

in which “ λ ” is the mean free path of a particular particle, “ d ” is the effective hard shell diameter of the particles which depends on the type of gas and is typically in the range of $2\text{--}6 \times 10^{-10}$ m (Gird 1994), “ k_B ” is the Boltzmann’s constant ($k_B = 1.38066 \times 10^{-23}$ J/K), and total gas pressure, “ p ”, and temperature, “ T ”, are expressed in Pa and K units, respectively.

The gas number density (i.e. the number of molecules per unit volume, “ n ”) of an ideal gas is related to the gas pressure and temperature, “ p ” and “ T ”, respectively, according to:

$$n = \frac{p}{k_B T} \quad (2)$$

Combining Eqs. 1 and 2 and considering the definition of Avogadro’s number (N_A), the mean free path of the ideal gas molecules can be calculated by:

$$\lambda = \frac{RT}{\sqrt{2} \pi d^2 N_A p} \quad (3)$$

As a result, the following relations could be used to calculate Knudsen number for an ideal gas:

$$Kn = \frac{RT}{\sqrt{2} \pi d^2 N_A p L} = \frac{1}{\sqrt{2} \pi d^2 n L} \quad (4)$$

Considering the case of air molecules within the vacuum chamber in our pore-scale SAGD visualization experiments, their associated mean free path increases as the

number of air molecules decreases in a unit volume. This increase in the mean free path increases Knudsen number; hence the continuum approach for predicting the thermal characteristics of air would not be applicable. If the mean free path of air molecules is in the order of, or greater than, the characteristic dimension of the problem in hand in our system (i.e. average distance of the micromodel from inner surface of the vacuum glass bell jar), the convective element of the heat transfer could be ignored. In other words, the convective heat transfer coefficient of the residual air phase within the vacuum chamber becomes insignificant.

Two optimistic and pessimistic scenarios were defined based on the maximum and minimum possible values of the mean free path for the air molecules inside the vacuum chamber considering the range of operating parameters provided in Table 3. If the mean free path of the air molecules is at maximum, the gas number density should be minimal. Minimum value of the gas number density could be attributed to operating the system at minimum vacuum pressure and maximum operating temperature. To obtain this most optimistic value for the mean free path of the air molecules, the calculations were conducted considering the lower range of the reported gas molecular size. In contrast, one can calculate the most pessimistic value (i.e. smallest possible value) of the mean free path of the air molecules by maximizing the number density (i.e. at maximum operating vacuum pressure and minimum experienced temperature) and assuming the upper range of the reported hard shell diameter for the gas molecules. Considering the calculated mean free path of the air molecules based on the operating conditions presented in Table 3, even the most pessimistic estimate (i.e. smallest value) of the mean free path is greater than the distance between the micromodel and inner side of the glass bell jar (i.e. 17–19 cm). It is concluded that the convective element of heat loss can be ignored within the range of operating conditions associated with our SAGD visualization experiments. In other words, the employed heat loss prevention technique was successful in minimizing the overall heat loss of the SAGD visualization experiments.

Table 3 Calculation of mean free path of air molecules within the vacuum chamber based on the operating conditions associated with the pore-scale SAGD experiments

Vacuum pressure inside the environmental chamber, torr	5×10^{-6} – 10^{-4}
Air temperature within the vacuum chamber, °C	34–44
Hard sphere diameter of air molecule, m	2×10^{-10} – 6×10^{-10}
Estimated mean free path, m	0.1989–36.9616

Details of the radiation heat loss analysis

Details of the heat loss analysis for our SAGD visualization experiments are presented based on the concept of radiation heat loss from a hot surface to the surrounding environment. This analysis was used to estimate the additional injection flux of water required to take care of the radiation heat loss. In addition, this analysis was used to design the heat loss experiments associated with our pore-scale SAGD trials. The problem statement is how to calculate the radiation heat loss from a hot inner surface enclosed in a much colder outer surface. The simplest example of an enclosure is one involving two surfaces that exchange radiation only with each other. Such a two-surface enclosure is shown schematically in Fig. 6.

Since there are only two surfaces, the net rate of radiation transfer from surface 1, q_1 , must be equal to the net rate of radiation transfer to surface 2, q_2 . The total radiation heat transfer between these two surfaces can be written in terms of the total resistance to radiation exchange between surfaces 1 and 2 which comprise the two surface resistances and the geometrical resistance. The net radiation exchange between surfaces can be expressed as (Incropera and DeWitt 2002):

$$q_{12}|_{\text{radiation}} = \left(\frac{1 - \varepsilon_1}{\varepsilon_1} + \frac{A_1 + A_2 - 2A_1F_{12}}{A_2 - A_1(F_{12})^2} + \left(\frac{1 - \varepsilon_2}{\varepsilon_2} \right) \frac{A_1}{A_2} \right)^{-1} \times A_1 \sigma (T_1^4 - T_2^4) \tag{5}$$

in which “ q_{12} ” is the net radiation exchange between the two surfaces, “ T_1 ” and “ T_2 ” are the temperature of surfaces 1 and 2, respectively, “ σ ” is the Stefan–Boltzmann constant, “ ε_1 ” and “ ε_2 ” are the emissivity of surfaces 1 and 2, respectively, “ A_1 ” and “ A_2 ” are the surface areas of surfaces 1 and 2, respectively, and “ F_{12} ” is the view factor.

A reasonable approximation of the arrangement of our glass micromodels inside an outer inverted glass bell jar could be presented in the form of a small convex object in a

large cavity. This enclosure of special diffuse gray surfaces is presented as one specific radiation mode in the literature and is formulated considering a series of assumptions (Incropera and DeWitt 2002). For instance, the area of the hot surface is considered to be negligible compared to that of the surrounding environment, hence $\frac{A_1}{A_2} \cong 0$. In addition, as the single hot spot is fully surrounded by the large cavity, the view factor, F_{12} , could be considered as unity. Subsequently, the net radiation heat loss between the hot and cold surfaces under these circumstances would be expressed as:

$$q_{12}|_{\text{radiation}} = \sigma A_1 \varepsilon_1 (T_1^4 - T_2^4) \tag{6}$$

The heat loss experiments were conducted using the same glass micromodels as those used in the pore-scale SAGD trials, but not in the presence of the oil phase, so the entire surface area of the micromodels were available to heat flow. Consequently, the calculated heat loss is based on the exposure of 100 % depleted model, filled with steam either at the saturation or superheated temperature, to the surrounding environment. This is the maximum possible heat loss during the pore-scale SAGD experiments and is equivalent to the case of 100 % recovery of initial oil in place. During each pore-scale SAGD trial, the amount of radiation heat loss was proportional to the invaded area of the model filled with steam at each particular depletion stage.

To calculate the total radiation heat loss from the hot surface of the glass micromodel to the colder surface of the glass bell jar, two optimistic and pessimistic scenarios are defined based on the operating conditions of the pore-scale SAGD experiments as well as those of the heat loss trials. The pessimistic radiation heat loss is calculated based on maximizing the total heat loss considering the range of operating conditions, assuming that the entire glass micromodel is filled with steam at its maximum experienced steady state superheating temperature, the glass jar temperature is at its minimum value, and maximum emissivity coefficient for the glass surface is considered. On the other hand, the minimum probable amount of the radiation heat loss (i.e. the optimistic value) can be calculated assuming that the glass micromodel is thoroughly filled with saturated steam, the glass bell jar temperature is at the maximum experienced value, and the emissivity coefficient for the glass surface is at the minimum amount based on the values proposed in the literature. Table 4 contains a summary of the calculation steps and results obtained.

At each particular recovery stage, the exposed area of the micromodel to the radiation heat loss is a fraction of the total surface area due to partial depletion of the model. Because the steady state operating temperature of each pore-scale SAGD test was kept relatively constant during

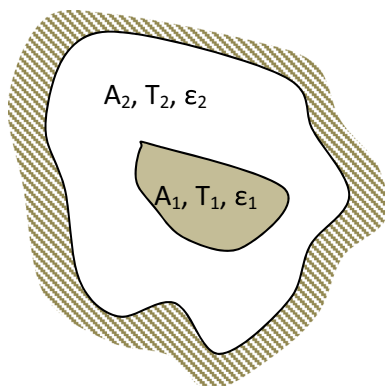


Fig. 6 The two-surface enclosure

Table 4 Radiation heat loss calculations for the employed glass micromodels in our SAGD visualization experiments based on the results obtained in the heat loss trials

Constants					
Stefan–Boltzmann constant (σ), $\frac{W}{m^2 K^4}$	5.670×10^{-8}				
Emissivity of glass micromodel surface (ϵ_1) at 300 K	0.90–0.95				
Glass micromodels	OC-1	DC-1	DL-1	OM-1	OM-2
Temperature range of the micromodel surface, °C	65–128	58–116	62–118	66–116	61–114
Temperature range of the glass bell jar of the vacuum chamber, °C	32–56	29–54	32–58	34–57	31–55
Model length, cm	35.00	35.00	35.10	35.60	35.60
Model width, cm	12.10	16.00	12.00	12.80	12.80
Total surface area, cm ²	847.00	1120	842.40	911.36	911.36
Pessimistic radiation heat loss, W	78.587	88.072	66.874	68.889	68.275
Optimistic radiation heat loss, W	33.067	45.341	31.650	34.914	36.240

each experiment, one can calculate the instantaneous heat loss by multiplying the maximum possible heat loss by the fraction of the model surface area which is exposed to the radiation heat loss. Details of this procedure is described later in the paper where the total cumulative steam consumed during each pore-scale SAGD trial was corrected for the amount of steam which condensed in the model to cover up for the heat loss to the surrounding.

Details of the heat and mass balance in the heat loss experiments associated with the pore-scale SAGD trials

One can write the overall heat and mass balance for the micromodel system to obtain how much volume of the water condensate during each particular run was originated only from the radiation heat loss. If this volume of the water condensate is subtracted from the total injected steam, it results in obtaining the volume of steam, in terms of CWE, required to facilitate the gravity-dominated process to the extent of achieving ultimate recovery factor values reported at the end of each particular SAGD trial. Hence, the energy intensity of each particular SAGD trial based on the steam requirements for each unit volume of the produced oil can be calculated. To achieve this goal, it is needed to calculate the maximum probable heat losses from the glass micromodel as was described in the previous section. Continuous tracking of the pore-scale SAGD interface helped to determine the ratio of the invaded area to the total area at each particular step during the SAGD process time. This enables us to calculate the cumulative water condensate produced due to the heat loss up until each particular drainage stage. For the heat loss experiments associated with the pore-level SAGD trials, one can write the overall heat balance for a system whose

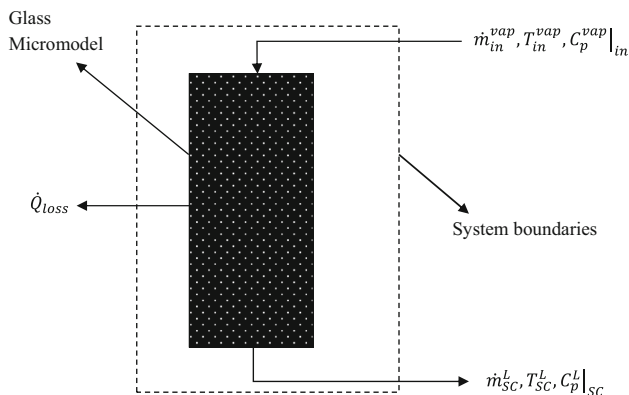


Fig. 7 Schematic flow diagram of a particular glass micromodel for the purpose of heat balance in the heat loss experiments

schematic flow diagram is presented in Fig. 7 with focus on the inlet and outlet mass and heat streams assuming that the convective element of the heat loss is negligible. One can write the conservation of enthalpy considering the inlet and outlet streams as:

$$H_{in} - H_{out} = \dot{Q}_{loss} \tag{7}$$

in which \dot{Q}_{loss} is the total heat loss from the model to the surrounding environment in the form of radiation heat loss, and H_{in} and H_{out} are the input and output enthalpies.

The input and output enthalpies can be expanded using a reference state enthalpy, so Eq. 7 could be written in the expanded form of:

$$\dot{m}_{in}^{vap} (H_{in}^{vap} - H_{ref.}^{vap}) = \dot{m}_{sc}^L (H_{sc}^L - H_{ref.}^{vap}) + \dot{Q}_{loss} \tag{8}$$

in which H_{in}^{vap} , H_{sc}^L , and $H_{ref.}^{vap}$ are the enthalpies associated with the inlet vapour phase, sub-cooled liquid condensate phase, and an arbitrary reference-state vapour phase at the corresponding temperatures, respectively. In addition, \dot{m}_{in}^{vap}

and \dot{m}_{SC}^L are the mass flow rates of the inlet steam phase and that of the outlet sub-cooled water condensate phase, respectively.

The mass balance over the system boundaries reveals that:

$$\dot{m}_{in}^{vap} = \dot{m}_{SC}^L = \dot{m} \tag{9}$$

in which the inlet vapour mass flow rate (\dot{m}_{in}^{vap}) is considered in terms of the equivalent cold liquid injection rate of the inlet phase.

Substituting Eq. 9 into Eq. 8 with some simplifications cancels out the terms containing the reference vapour phase enthalpy from both sides of the equality, and leads to the following simple form of:

$$\dot{m}(H_{in}^{vap} - H_{SC}^L) = \dot{Q}_{loss} \tag{10}$$

Adding and subtracting a “ $\dot{m}H_{sat}^{vap}$ ” into the LHS of Eq. 10 results in:

$$\dot{m}(H_{in}^{vap} - H_{sat}^{vap}) + \dot{m}(H_{sat}^{vap} - H_{SC}^L) = \dot{Q}_{loss} \tag{11}$$

Considering the fact that $H_{sat}^{vap} = H_{sat}^L + \lambda$, Eq. 11 leads to:

$$\dot{m}(H_{in}^{vap} - H_{sat}^{vap}) + \dot{m}(H_{sat}^L - H_{SC}^L) + \dot{m}\lambda = \dot{Q}_{loss} \tag{12}$$

in which λ is the enthalpy of condensation at the operating pressure condition and H_{sat}^{vap} is the enthalpy of the vapour phase at the saturation temperature corresponding to the overall operating pressure.

Expanding the enthalpy parameters in terms of specific heat capacities and temperatures converts Eq. 12 into a more broadly used format of:

$$\dot{m}\left(C_p^{vap}\Big|_{in} T_{in}^{vap} - C_p^{vap}\Big|_{sat} T_{sat}^{vap}\right) + \dot{m}\left(C_p^L\Big|_{sat} T_{sat}^L - C_p^L\Big|_{SC} T_{SC}^L\right) + \dot{m}\lambda = \dot{Q}_{loss} \tag{13}$$

in which T_{in}^{vap} , T_{sat}^{vap} , T_{sat}^L , and T_{SC}^L are the superheated vapour temperature at the inlet side, saturated vapour temperature at the corresponding operating pressure, saturated liquid temperature at the corresponding operating pressure, and temperature of the sub-cooled liquid phase at the outlet side, respectively. Moreover, the average specific heat capacity values of liquid and vapour phases are defined based on their associated stream temperatures.

If the rate of change of the specific heat versus temperature would be close to linear, the magnitude of the specific heat at average temperature could be used:

$$\dot{m}C_p^{vap}\Big|_{\frac{T_{in}^{vap}+T_{sat}^{vap}}{2}}(T_{in}^{vap} - T_{sat}^{vap}) + \dot{m}C_p^L\Big|_{\frac{T_{SC}^L+T_{sat}^L}{2}}(T_{sat}^L - T_{SC}^L) + \dot{m}\lambda\Big|_{T_{sat}} = \dot{Q}_{loss} \tag{14}$$

Otherwise if “ C_p ” variation versus temperature was not linear, one should calculate the area under the curve for specific heat capacity versus temperature plot:

$$\int_{T_{sat}^{vap}}^{T_{in}^{vap}} \dot{m}C_p^{vap}dT + \int_{T_{SC}^L}^{T_{sat}^L} \dot{m}C_p^LdT + \dot{m}\lambda\Big|_{T_{sat}} = \dot{Q}_{loss} \tag{15}$$

According to steam table, the isobaric specific heat capacity of steam at the operating temperature range of our SAGD visualization experiments changes linearly with temperature which satisfies use of Eq. 14 to calculate the overall heat transfer of the process. This equation is written below based on the fluids present in the heat loss experiments associated with the SAGD flow system:

$$\dot{m}C_p^s\Big|_{\frac{T_{in}^s+T_{sat}^s}{2}}(T_{in}^s - T_{sat}^s) + \dot{m}C_p^w\Big|_{\frac{T_{SC}^w+T_{sat}^w}{2}}(T_{sat}^w - T_{SC}^w) + \dot{m}\lambda\Big|_{T_{sat}} = \dot{Q}_{loss} \tag{16}$$

in which “ T_{in}^s ” is the superheated steam temperature at the inlet side, “ T_{sat}^s ” is the saturated steam temperature at the corresponding operating pressure, “ $C_p^s\Big|_{\frac{T_{in}^s+T_{sat}^s}{2}}$ ” is the specific heat capacity of steam at a temperature equivalent to the average of superheated steam temperature at the inlet side and that of the saturated steam at the corresponding operating pressure, “ $C_p^w\Big|_{\frac{T_{SC}^w+T_{sat}^w}{2}}$ ” is the water condensate specific heat capacity at a temperature equivalent to the average of sub-cooled water temperature at the outlet side and that of the saturated water phase at the corresponding operating pressure, “ T_{sat}^w ” is the saturated water condensate temperature at the corresponding operating pressure, and “ T_{SC}^w ” is the temperature of the sub-cooled water condensate phase at the outlet side.

One can isolate the mass flux of water required to satisfy the radiation heat loss:

$$\dot{m} = \frac{\dot{Q}_{loss}}{\left\{ C_p^s\Big|_{\frac{T_{in}^s+T_{sat}^s}{2}}(T_{in}^s - T_{sat}^s) + C_p^w\Big|_{\frac{T_{SC}^w+T_{sat}^w}{2}}(T_{sat}^w - T_{SC}^w) + \lambda\Big|_{T_{sat}} \right\}} \tag{17}$$

in which “s” denotes the steam phase and “w” represents the water phase, and \dot{m} is the mass flow rate of steam, in terms of injected CWE, taking care of the radiation heat loss.

Table 5 presents the parameters required to calculate the mass flux of water, which is needed to take care of the radiation heat loss using Eq. 17. For each particular micromodel, range of the steam temperature was considered from the dry saturated steam temperature (100 °C) to maximum experienced superheating temperature. Two different scenarios were defined to calculate the maximum and minimum required water mass influx to compensate for the radiation heat loss for each particular glass micromodel. In an optimistic scenario, the minimum amount of

Table 5 Maximum required mass flux of steam, in terms of CWE, to cover for the radiation heat losses in the heat loss experiments based on two optimistic and pessimistic scenarios

	OC-1	OM-1	DC-1	DL-1	OM-2
Steam temperature range, °C	100 to 128	100 to 116	100 to 116	100 to 118	100 to 114
Water condensate temperature range, °C	86 to 100	83.6 to 100	84 to 100	84.5 to 100	83 to 100
$\dot{m} _{\text{pessimistic}}$, g/min	1.987	1.752	2.241	1.700	1.737
$\dot{m} _{\text{optimistic}}$, g/min	0.856	0.900	1.170	0.817	0.933

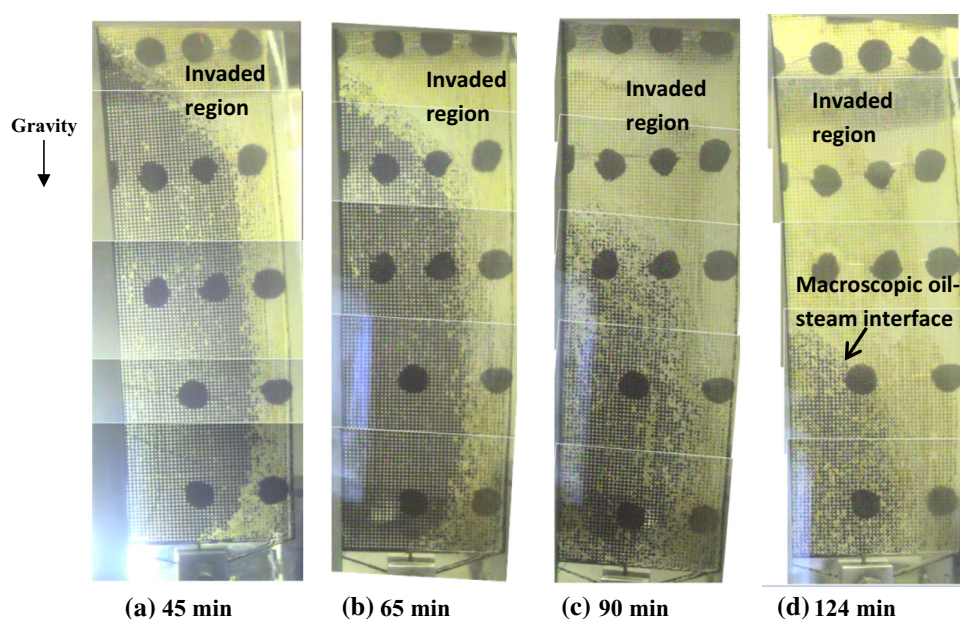
water mass influx is calculated in such a way that the model is assumed to be at the lowest possible operating temperature. However, a pessimistic scenario was defined to express the greatest magnitude of the water influx required to compensate for the radiation heat loss if the superheated steam was injected into the model. All the heat loss experiments were carried out under atmospheric conditions of operating pressure. The values presented in the last two rows of Table 4 give us a feel on how much steam should be delivered to the system while operating in the SAGD mode. These calculations also helped us to design the actual pore-scale SAGD experiments using the data obtained during the heat loss calculations.

Determination of energy requirements of the pore-scale SAGD experiments using heat loss analysis and pore-level interface tracking

A total of seven pore-scale SAGD experiments were considered in this paper for the purpose of obtaining the true energy requirements accounting for the energy loss through radiation heat losses. The volumetric measurements carried

out during these pore-scale SAGD experiments were used to determine the energy requirements of the SAGD process in terms of the net CSOR. The cumulative amount of water produced in each SAGD experiment was measured during different stages of the process such as start-up stage, early development of the steam chamber, and chamber propagation stage. The instantaneous steam injection rate, in terms of CWE, was slightly adjusted during the process time to achieve a relatively constant steam temperature in the invaded area of the porous pattern in the presence of continuously growing heat loss. The cumulative steam injected during each particular SAGD trial was obtained by multiplying the instantaneous steam injection rate by time duration over which each particular injection rate was maintained constant. There was a good agreement between the cumulative water produced and the cumulative steam injected during every stage of the SAGD trials. The instantaneous SAGD interface position along the height of each micromodel was determined for each particular SAGD trial. A sample of the SAGD interface advancement versus time for model DL-1 in one of our visualization experiments is presented in Fig. 8. Using such an interface advancement pattern, it is possible to calculate the invaded

Fig. 8 SAGD interface advancement in RUN No. 8 (Model DL-1)



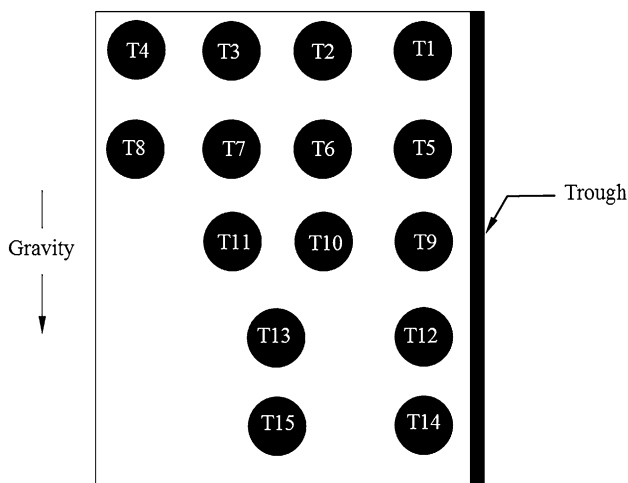


Fig. 9 The distribution of surface thermocouples along the height of Model DL-1 in RUN No. 8 of the SAGD visualization experiments

area of each glass micromodel during particular stages of the SAGD process. Considering the fraction of area swept per total area and the heat loss calculations performed previously, the contribution of the produced water condensate, originated from the heat loss, in the cumulative steam injected was determined at the end of each particular pore-scale SAGD experiment.

For the purpose of heat loss calculations, it is needed to carefully monitor the temperature of the glass micromodels, especially the swept area, during the pore-scale SAGD experiments. Thermocouples were attached to the glass surface of the micromodels to provide a real-time temperature map during each particular SAGD experiment. For instance, in RUN No. 8 in which DL-1 Model was used, 15 thermocouples were attached to the surface of the glass micromodel. The distribution of the surface thermocouples in this test is schematically shown in Fig. 9. The real-time temperature data were collected using an automated data acquisition unit. The temperature contour map at 4 selected intervals during this test is also shown in Fig. 10. According to the thermocouple arrangement displayed in Fig. 9, it is evident that thermocouples T1, T2, T3 and T4, which were located at the top row within the first 1–30 pores from the top of Model DL-1, as well as thermocouples T5, T9, T12 and T14, which were attached adjacent to the trough on the most right hand side column of the thermocouples, show early development of the steam chamber while other thermocouples show significantly lower local temperature values, close to the initial temperature of the glass micromodel.

The net CSOR can be calculated using net cumulative steam consumed and the cumulative oil produced in each particular SAGD trial. The net CSOR values of seven pore-scale SAGD tests were calculated/compared to each other

in this section to analyze their associated energy requirements. In Table 6, a summary of the runs information as well as the net CSOR values is presented. Using the procedure stated above to calculate the instantaneous heat losses from the micromodel, the cumulative amount of steam required to cover the heat losses was calculated for each particular pore-scale SAGD experiment. The net amount of steam needed to facilitate the gravity drainage process was then calculated by subtracting the cumulative volume of steam needed to provide for the heat losses from the total cumulative steam injected. The net CSOR values were then calculated by dividing the net cumulative steam volume consumed by the cumulative mobile oil produced. Focusing on RUN No’s 1 and 4 in Table 6 in which OM-1 model was used as the porous medium at two different degrees of steam superheat, it is observed that the net CSOR value is reduced by almost 63 % as a result of 14.70 °C increase in the steam temperature. The same conclusion can also be made considering RUN No’s 2 and 5 in which OM-2 model was employed. It is evident that following 7 °C increase in the operating temperature, the net CSOR value was decreased by about 22 %. It is concluded that the greater the operating temperature of the SAGD process, the smaller the associated value of the net CSOR.

The energy requirements of the pore-scale SAGD tests were also validated using application of gravity drainage theory in the SAGD recovery process. A conceptual model was originally proposed by Butler et al. (1979, 1981) and was developed further through subsequent publications (Butler and Stephens 1981; Butler 1991, 1994a, b) to estimate the drainage rate of the mobile oil under the SAGD process. According to this theory, the mobile oil drainage rate as well as the steam chamber interface velocity in the horizontal direction is affected by reservoir rock and fluid properties. The horizontal advancement velocity of the SAGD interface is expressed in the form of:

$$q = \sqrt{\frac{2\phi\Delta S_o k g \alpha (h - y)}{m v_s}} \tag{18}$$

in which “*q*” is the mobile oil production rate, “*k*” and “*ϕ*” are reservoir permeability and porosity, respectively, “*g*” is the gravitational acceleration, “*v_s*” is the oil kinematic viscosity at steam temperature, “*ΔS_o*” is the change in oil saturation following the SAGD process, “*h*” is the reservoir height, and “*m*” is an empirical parameter.

To present the net CSOR data associated with RUN No’s 1–7 using a single scaled graph, it is required to define a scaling coefficient to accommodate for variations in experimental variables such as permeability, porosity, and operating temperature. It was found that when pore-scale SAGD tests were conducted in models with the same

Fig. 10 Temperature contour map during RUN No. 8 of the SAGD visualization experiments

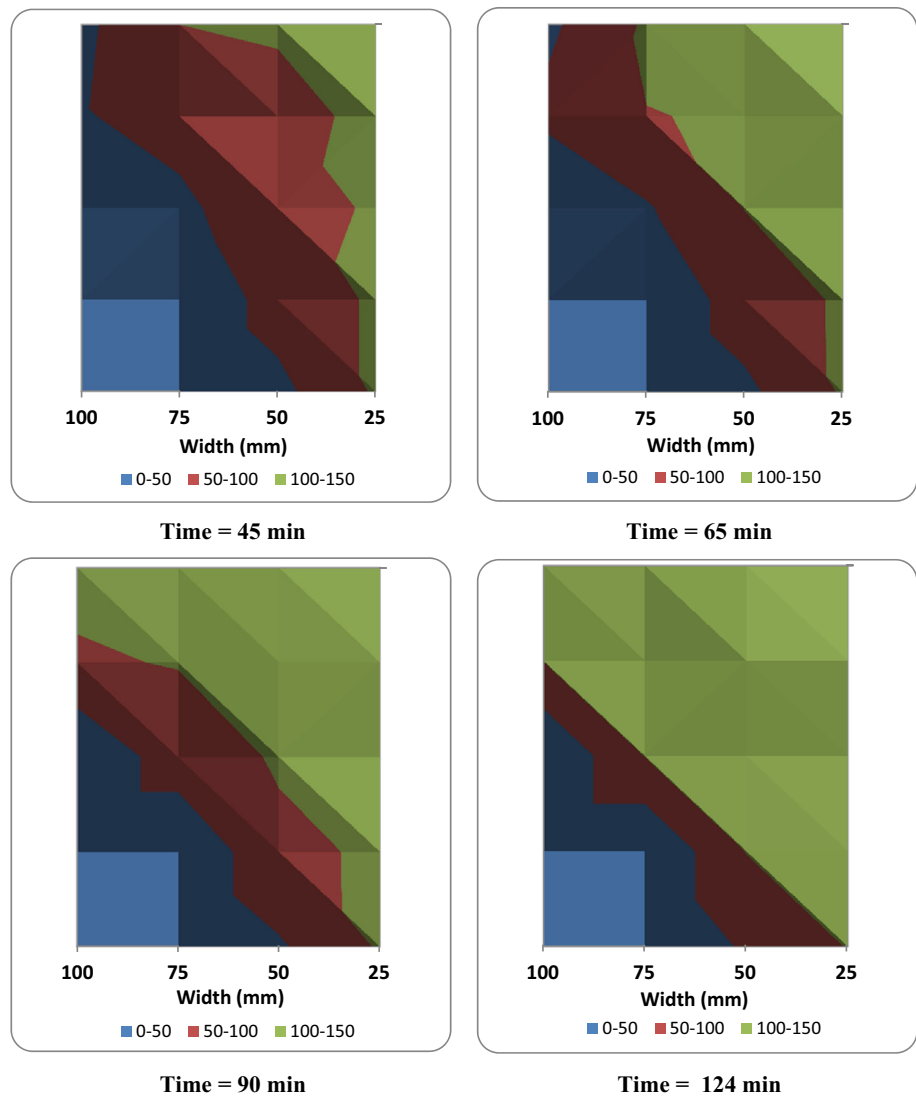


Table 6 Energy requirements calculations for the pore-level SAGD experiments

Run no.	Model	Runtime (min)	Average operating temperature (°C)	Cum. oil produced (cm ³)	Cum. steam injected (cm ³ of CWE)	Cum. steam needed for heat loss (cm ³ of CWE)	Net steam consumed (cm ³ of CWE)	Net CSOR
6	OC-1	230	101.20	1.11	81.95	70.75	11.20	10.05
7	DC-1	400	102.40	0.66	95.17	86.38	8.79	13.28
3	DL-1	175	103.10	1.92	77.20	65.88	11.32	5.90
1	OM-1	210	101.70	0.78	74.75	67.54	7.21	9.20
2	OM-2	205	103.40	1.34	78.82	70.83	7.99	5.97
4	OM-1	120	116.35	0.79	51.55	47.07	4.48	5.66
5	OM-2	140	110.20	1.30	54.97	48.61	6.36	4.91

thermal properties and bitumen type, the net CSOR values are proportional to the square root of kinematic oil viscosity at the steam temperature and are also inversely proportional to the square root of porosity multiplied by

permeability assuming that all other experimental variables remain unchanged. Table 7 contains some data associated with the pore-level SAGD experiments including operating conditions, model properties, and calculated net CSOR

Table 7 Parameters affecting the net CSOR values of the pore-level SAGD experiments based on the gravity drainage theory and the SAGD visualization experiments

Run no.	Model	k (D)	ϕ (fraction)	T_s (°C)	μ at T_s (cP)	ρ at T_s (g/cc)	v @ T_s (cSt)	Net CSOR (vol/vol)	$\sqrt{\frac{k\phi}{v_s}}$ ($\times 10^{-3} \text{ s}^{1/2}$)
3	DL1	94.61	0.32	103.10	243.425	0.957	254.405	5.90	0.345
2	OM2	92.42	0.32	103.40	240.431	0.957	251.321	5.97	0.343
1	OM1	77.83	0.30	101.70	258.023	0.958	269.435	9.20	0.294
7	DC1	34.13	0.37	102.40	250.593	0.957	261.786	13.28	0.220
6	OC1	56.16	0.42	101.20	263.497	0.958	275.069	10.05	0.293
5	OM2	92.42	0.32	110.20	183.300	0.953	192.386	4.91	0.392
4	OM1	77.83	0.30	116.35	145.445	0.949	153.219	5.66	0.390

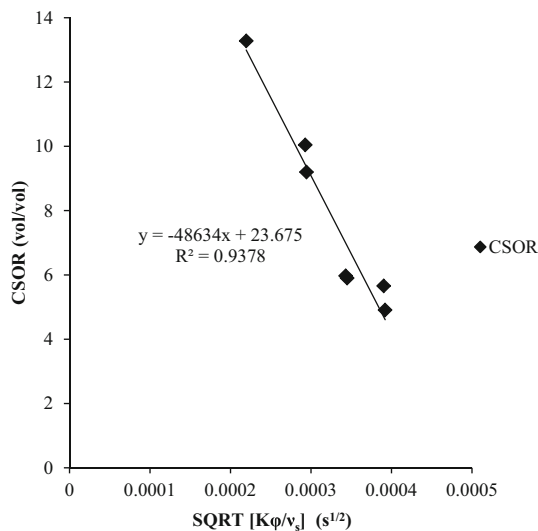


Fig. 11 Net CSOR values versus the correlation coefficient for SAGD RUN No’s 1–7

values. The last column in Table 7 is the scaling parameter by which all the net CSOR data associated with all 7 of the SAGD tests were collapsed into a single graph as is depicted in Fig. 11. All the net CSOR values fit reasonably into a single graph regardless of their associated variabilities such as differences in the porous media properties as well as operating temperature. The proposed scaling parameter is able to provide a very good correlation with diverse range of the net CSOR values when all other experimental variables remain unchanged.

Conclusions

A novel method for heat loss prevention during the course of in situ bitumen recovery using the SAGD process was utilized with the aid of a high-precision inverted-bell vacuum chamber. This method was effective in diminishing the convective heat transfer mechanism of thermal

energy losses from the porous media at elevated temperatures of superheated steam. Heat loss experiments were conducted to determine the maximum possible heat losses, facilitated with the radiation heat transfer mechanism, at corresponding operating conditions when there was no oil in the micromodels. Fractional instantaneous heat losses from the porous media under radiation heat transfer mechanism were calculated during the actual pore-scale SAGD experiments considering the fraction of the swept area of glass micromodels, real-time bitumen-steam interface tracking, and energy dissipation calculations using information derived from the heat loss experiments. The analysis of heat loss was an integrated part of calculating the net CSOR values to correct the total amount of consumed thermal energy for the volume of steam which was consumed to cover the radiation heat loss. The net CSOR values signify the actual thermal energy needed to mobilize the in situ bitumen under pertaining operating conditions. The net CSOR data were validated using the theory of gravity drainage and its application in the SAGD process. A scaling parameter was defined based on this theory to correlate the net CSOR values with the experimental variables. An acceptable linear correlation was obtained by plotting all the net CSOR data versus this scaling parameter over the entire range of the experimental variables.

Acknowledgments The financial support of this research, provided by the Natural Sciences and Engineering Research Council of Canada (NSERC) is gratefully acknowledged. The authors would like to express their gratitude to the Micro-Electronics and Heat Transfer Laboratory (MHTL), University of Waterloo, especially Professor Richard Culham (MHTL Director) and Professor Pete Teertstra, for providing continuous support during the course of the visualization studies.

Open Access This article is distributed under the terms of the Creative Commons Attribution 4.0 International License (<http://creativecommons.org/licenses/by/4.0/>), which permits unrestricted use, distribution, and reproduction in any medium, provided you give appropriate credit to the original author(s) and the source, provide a link to the Creative Commons license, and indicate if changes were made.

References

- Butler RM (1987) Rise of interfering steam chamber. *J Can Petrol Technol* 26(3):70–75
- Butler RM (1991) Thermal recovery of oil and bitumen. Prentice Hall, Englewood Cliffs
- Butler RM (1994a) Steam-assisted gravity drainage: concept, development, performance, and future. *J Can Pet Technol* 32(2):44–50
- Butler RM (1994b) Horizontal wells for the recovery of oil, gas and bitumen. In: Petroleum Society monograph number 2. Canadian Institute of Mining Metallurgy and Petroleum, Westmount
- Butler RM (1998) SAGD comes of age! *J Can Pet Technol* 37(7):9–12
- Butler RM (2001) Some recent developments in SAGD. *J Can Pet Technol* 40(1):18–22 (**JCPT Distinguished Author Series**)
- Butler RM (2004) The behaviour of non-condensable gas in SAGD—a rationalization. *J Can Petrol Technol* 43(1):28–34
- Butler RM, Stephens DJ (1981) The gravity drainage of steam heated heavy oil to parallel horizontal wells. *J Can Pet Technol* 20:90–96
- Butler RM, McNab GS, Lo HY (1979) Theoretical studies on the gravity drainage of heavy oil during in situ steam heating. Presented at the 29th Canadian chemical engineering conference, Sarnia, ON, 1–3 October
- Butler RM, McNab GS, Lo HY (1981) Theoretical studies on the gravity drainage of heavy oil during in situ steam heating. *Can J Chem Eng* 59:455–460
- Gird G (1994) Molecular gas dynamics and the direct simulation of gas flows. Clarendon Press, Oxford
- Guyer EC (1999) Handbook of applied thermal design, 1st edn. CRC Press, New York
- Incropera FP, DeWitt DP (2002) Fundamentals of heat and mass transfer, 5th edn. Wiley, New York. ISBN 0-471-38650-2
- Mohammadzadeh O (2012) Experimental studies focused on the pore-scale aspects of heavy oil and bitumen recovery using the steam assisted gravity drainage (SAGD) and solvent-aided SAGD (SA-SAGD) recovery processes. PhD dissertation, University of Waterloo
- Mohammadzadeh O, Chatzis I (2010) Pore-level investigation of heavy oil recovery using steam assisted gravity drainage (SAGD). *J Oil Gas Sci Technol* 65(6):839–857. doi:[10.2516/ogst/2010010](https://doi.org/10.2516/ogst/2010010)
- Mohammadzadeh O, Rezaei N, Chatzis I (2010) Pore-level investigation of heavy oil and bitumen recovery using solvent-aided steam assisted gravity drainage (SA-SAGD) process. *ACS J Energy Fuels* 24:6327–6345. doi:[10.1021/ef100621s](https://doi.org/10.1021/ef100621s)
- Mohammadzadeh O, Rezaei N, Chatzis I (2012) Production characteristics of the steam-assisted gravity drainage (SAGD) and solvent-aided SAGD (SA-SAGD) processes using a 2-D macroscale physical model. *ACS J Energy Fuels* 26:4346–4365. doi:[10.1021/ef300354j](https://doi.org/10.1021/ef300354j)
- Mohammadzadeh O, Rezaei N, Chatzis I (2015) Pore-scale performance evaluation and mechanistic studies of the solvent aided SAGD (SA-SAGD) process using visualization experiments. *Transp Porous Media* 108(2):437–480. doi:[10.1007/s11242-015-0484-y](https://doi.org/10.1007/s11242-015-0484-y)
- Roth A (1990) Vacuum technology, 3rd edn. North-Holland, Amsterdam